Solid State Phenomena
ISSN: 1662-9779, Vol. 390, pp 85-96
doi:10.4028/p-S75TgF

Submitted: 2026-01-16
Revised: 2026-02-13
Accepted: 2026-02-21
Online: 2026-04-17

Modeling Transient Temperature-Driven Microstructure Evolution in Inconel 718 during Hot Forming

Nadine ELEKYABI[1,a], Holger BRÜGGEMANN[1,b], Emad SCHARIFI[1,c*] and Junhe LIAN[1,c]

[1]Institute of Metal Forming (IBF), RWTH Aachen University, Germany

[a]nadine.elekyabi@ibf.rwth-aachen.de, [b]holger.brueggemann@ibf.rwth-aachen.de, [c]emad.scharifi@ibf.rwth-aachen.de, [d]junhe.lian@ibf.rwth-aachen.de

*corresponding author

Keywords: Superalloys, Non-isothermal Deformation, Microstructure Modeling, Hot Forming

Abstract. Industrial hot forming of nickel-based superalloys is typically carried out under non-isothermal conditions, where rapid temperature changes between forming steps not only affect the thermo-mechanical response but also the microstructural evolution, including processes such as recrystallization. Most microstructure models are developed and calibrated for idealized isothermal conditions, and their applicability to realistic transient temperature paths is still unclear. Therefore, this study investigates the microstructure evolution of Inconel 718 under non-isothermal hot deformation by combining dilatometer tests with full-field simulations using DIGIMU® in order to provide detailed insight into the underlying microstructural mechanisms and to assess the capability of a Full-Field approach for modelling such non-isothermal forming conditions. For this aim, compression tests with temperature increases (1020 °C to 1070 °C) and decreases (1120 °C to 1070 °C) were performed, with the temperature change applied at different strains.
The results reveal a path dependence, heating at low strain to 1070 °C leads to higher DRX-fractions and finer, more homogeneous grain structures, whereas later heating at higher strains produces coarser, partially recrystallized microstructures due to reduced strain at the higher temperature. For the temperature decrease, DRX occurs predominantly at 1120 °C, after a late temperature change, no additional DRX takes place at 1070 °C. While an earlier change still allows additional DRX. The Full-Field simulations reproduce these trends in dislocation density, recrystallized fraction and grain size distributions with good qualitative agreement and moderate quantitative deviations.

Overall, the study demonstrates that the timing and direction of temperature changes affect the final microstructural state, and that DIGIMU®, a Full-Field approach, can capture path-dependent microstructure evolution in Inconel 718 and provides a useful digital tool for analyzing and designing transient temperature hot forming processes.

Introduction

Hot forming is a central manufacturing route for producing high-performance components with tailored mechanical properties. During such processes, the microstructure evolves continuously through mechanisms such as work hardening, dynamic recovery, dynamic recrystallization (DRX), post-dynamic recrystallization (PDRX) and grain growth [1,2]. Because these mechanisms control grain structure and, in turn, mechanical properties, it is essential to study the microstructural evolution during hot deformation. The resulting microstructure evolution and the kinetics of these mechanisms are closely linked to the process parameters such as strain rate, deformation temperature and deformation degree [3,4].

Nickel-base superalloys, such as Inconel 718, which are widely used in aircraft engines and energy applications because of their excellent high temperature properties [5], are a prominent example where this microstructure sensitivity is critical. As a result, their hot deformation behavior and microstructural evolution have been investigated in numerous works [6–8].
In these works, the temperature histories are typically idealized as constant values. In real hot forming processes, however, the thermal conditions are often non-isothermal. In open-die forging, for

example, after each form passes, an increase and decrease of the core temperature of the material is observed [9]. As a result, the material experiences transient heating and cooling during ongoing deformation, which can modify the competition between hardening, recovery and recrystallization compared with idealized isothermal processes. Lin et al. [10] investigated non-isothermal two-stage hot deformation of a Ni-Fe-Cr base superalloy and showed that with different final deformation temperatures, strain rates and first-stage strains lead to different DRX fractions. However, their study is purely experimental and limited to global quantities in the final states after the experiment, without access to intermediate microstructural states.

To analyze such conditions in more detail, Full-Field models are required that enable the detailed tracking of microstructural states throughout the deformation process. This approach improves the link between process parameters and microstructural changes, since every intermediate state can be analyzed without additional experimental effort [11]. In this work, the Full-Field framework DIGIMU® is used for that purpose. It is designed to simulate multistage hot forming processes within reasonable computation times and to model microstructural evolution at the grain level on a meshed representative volume element (RVE) containing multiple grains. The framework uses an explicit grain structure and uses experimentally derived boundary conditions, such as temperature-time histories and strain rate, to reproduce realistic deformation conditions. Grain boundary migration and recrystallization are described by a finite element formulation coupled with a level-set approach, which allows grain boundaries to move in response to curvature and differences in stored energy between neighboring grains. The underlying kinetic models account for the coupled evolution of dislocation density, grain boundary migration and recrystallization, including dynamic recrystallization (DRX) and post-dynamic recrystallization (PDRX) [12–14].

This study therefore addresses the mentioned gap by combining transient hot compression tests on Inconel 718 with Full-Field simulations in DIGIMU®, using the experimentally measured time-temperature histories as boundary conditions to assess the model's ability to reproduce and analyze the microstructural evolution under transient temperatures. In this way the microstructural behavior is studied under process-relevant thermal conditions that are close to those encountered in industrial hot forming, while allowing the microstructure to be analyzed at arbitrary points in time during the deformation.

Materials and Methods

Material. The investigated material is an industrially produced wrought bar of the nickel-based superalloy Inconel 718. The initial stock with a diameter of 160 mm was forged in ten passes to a rectangular cross-section of 87 mm x 87 mm. After forging, the material was solution annealed at 1030 °C for 1 h. The chemical composition of used Inconel 718 is given in Table 1.

Table 1. Chemical composition of the investigated Inconel 718 alloy [wt.%]

C	Si	Mn	P	S	Cr	Ni	Mo
0.022	0.06	0.08	0.007	0.0004	17.63	53.9	2.97
Al	Ti	Co	Cu	Nb	Fe	B	Ta
0.52	0.94	0.32	0.04	4.98	18.49	0.0024	<0.02

Experimental Procedure. Non-isothermal hot compression tests were carried out to determine the material behavior under changing temperatures. All tests were conducted on cylindrical Inconel 718 specimens with dimensions 5 mm in diameter and 10 mm in height, using a quenching and deformation dilatometer DIL 805 (TA Instruments).

In this device, the specimens are inductively heated and the temperature is controlled by a thermocouple welded directly to the specimen surface. The dilatometer allows testing in a temperature range from room temperature up to 1500 °C. It is equipped for compression tests with a maximum forming force of 20 kN, enabling strain rates between 0.001 s^{-1} and 20 s^{-1} and strains up to 1.2, which covers the deformation conditions investigated in the present study. The schematic experimental procedure for the non-isothermal hot compression tests is illustrated in Figure 1 for the

case of temperature decrease. For each transient temperature test, the specimen was first heated at a rate of 10 K/s to the desired initial deformation temperature T_1 and held for 30 s to minimize temperature gradients. The first deformation was carried out at T_1 up to a predefined strain ε_1. After this the temperature was changed to a second deformation temperature T_2 and the deformation was continued to the final strain ε_2.

Two types of non-isothermal tests were performed. Tests with a temperature increase from 1020 °C to 1070 °C and tests with a temperature decrease from 1120 °C to 1070 °C. In both series, the temperature change was imposed at different true strain levels ($\varepsilon = 0.2$, 0.4 and 0.6) in order to cover both the hardening dominated regime and the softening regime of the flow curve. The complete experimental matrix, including the combinations of initial temperature, temperature path and strain level at which the temperature change was applied, is summarized in Table 2. In addition, isothermal tests at constant temperatures of 1020 °C, 1070 °C and 1120 °C were also carried out as reference experiments up to a strain of 0.8. After deformation, all specimens were rapidly quenched with argon gas in order to freeze the microstructure. Subsequently, all specimens were metallographically prepared (grinding, polishing and etching). Microstructural images were taken with optical microscopy and the grain size was evaluated using the line-intercept method in accordance with DIN EN ISO 643 [15].

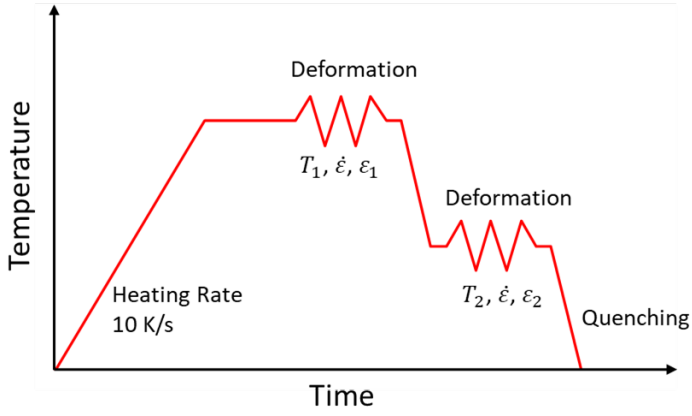

Fig.1. Schematic procedure of the transient temperature hot compression tests

Table 2. Experimental matrix of hot compression tests

Temperature T_1 [°C]	Temperature T_2 [°C]	Strain rate $\dot{\varepsilon}$ [s^{-1}]	Changing rate [°C/s]	Switching strain ε
1020	1070	0.1	100	0.2
1020	1070	0.1	100	0.4
1020	1070	0.1	100	0.6
1120	1070	0.1	100	0.2
1120	1070	0.1	100	0.4
1120	1070	0.1	100	0.6

During all transient tests, the temperature-time history of the specimen was recorded continuously by the welded thermocouple. As an example, Figure 2 shows one measured temperature evolution for the heating path from 1020 °C to 1070 °C and one for the cooling path from 1120 °C to 1070 °C. From these curves, effective heating and cooling rates of about 100 K/s were determined in the temperature change stage, demonstrating that the dilatometer is capable of achieving such rapid transient temperature changes during hot compression. These experimentally measured temperature histories were used directly as thermal boundary conditions in the DIGIMU® simulations described in the following section in order to reproduce the non-isothermal deformation conditions as realistically as possible.

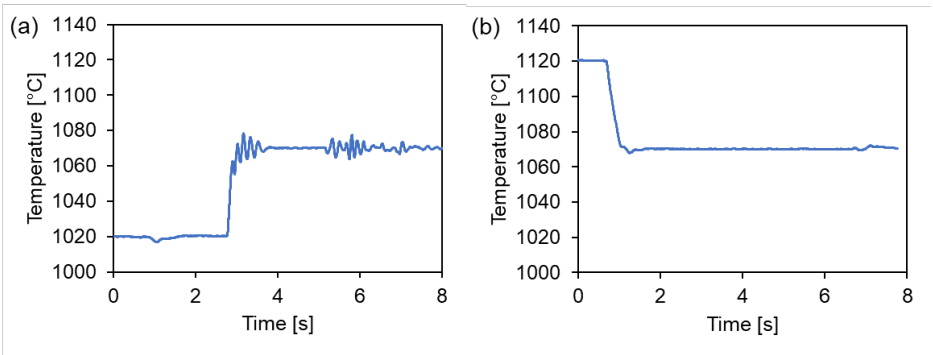

Fig. 2. Representative measured temperature-time histories of the specimen during transient temperature tests for a) a temperature increase from 1020 °C to 1070 °C at $\varepsilon = 0.2$ and b) a temperature decrease from 1120 °C to 1070 °C at $\varepsilon = 0.2$

Simulation Setup. To generate a representative polycrystalline RVE with a lognormal grain size distribution in DIGIMU®, statistical grain size information from the initial microstructure was used. The starting microstructure of the solution-annealed material was characterized by light optical microscopy, and the grain size distribution was quantified using the line-intercept method [15]. From these measurements, the grain size distribution within a given section was determined. Based on these parameters, a polycrystalline RVE containing 50 grains and following a lognormal grain size distribution was generated. The initial microstructure is shown in Figure 3 and the corresponding grain size distribution is listed in Table 3. The material parameters used in the Full-Field model were based on the parametrization in [16] investigations, in which the hot deformation response of Inconel 718 through four key mechanisms is captured: grain growth, dynamic hardening and recovery, dynamic recrystallization (DRX), and post-dynamic recrystallization (PDRX). This parameter set was adapted for use in the framework of DIGIMU® 5.0. The boundary conditions were defined in analogy to the experimental tests. The temperature evolutions were directly taken from the experimentally measured temperature-time histories T(t) as shown in Figure 2 and Table 2. The simulations were carried out under a constant strain rate of 0.1 s^{-1}, and up to a strain of $\varepsilon = 1$, which corresponds to the local strain levels in the center of the specimen when accounting for barreling [17].

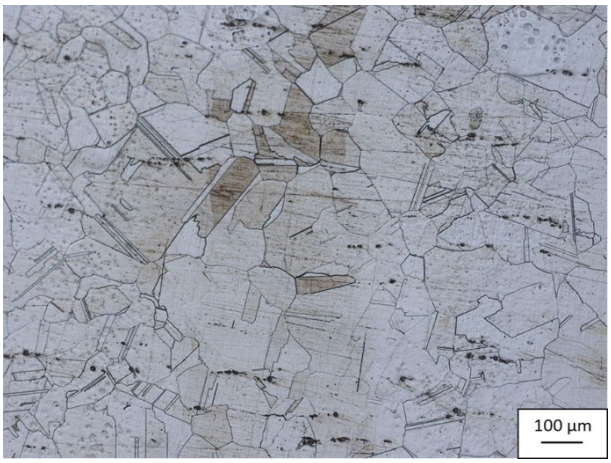

Fig. 3. Initial microstructure of Inconel 718

Table 3. Grain size distribution of initial RVE of Inconel 718

Mean grain size [µm]	Standard deviation	Min. grain size [µm]	Max. grain size [µm]
89.9	65.0	10.2	435.4

Results and Discussion

Evolution of Dislocation Density under transient temperatures with DIGIMU®. Figure 4 illustrates the evolution of the mean dislocation density $\bar{\rho}$ together with the critical dislocation density ρ_{cr} used in the DIGIMU® model. DRX is triggered once $\bar{\rho}$ exceeds ρ_{cr}. Panel (a) shows the results for temperature increase from 1020 °C to 1070 °C with switches at equivalent strains in the specimen center ε_{eq} = 0.2, 0.4 and 0.6, while panel (b) presents the corresponding temperature decreases from 1120 °C to 1070 °C. In the heating cases (Figure 4 (a)) the changing temperature curves (black), initially follow the isothermal reference $T_1 = 1020\,°C$ up to the switch strain. For the earliest switch at $\varepsilon_{eq} = 0.2$, the temperature change takes place before $\bar{\rho}$ reaches the critical value of the 1020 °C reference ρ_{cr} = 4.8E+08 mm^{-2} (upper dashed line). At the moment of the change, the material has therefore not entered the DRX regime corresponding to 1020 °C. The microstructure is still dominated by dynamic hardening. When the temperature is raised to 1070 °C, ρ_{cr} drops to 3.5E+08 mm^{-2} (lower dashed line), so that the current $\bar{\rho}$ lies above the new critical value and DRX is activated immediately after the change at $\varepsilon_{eq} = 0.25$. The dislocation density curve gradually adapts to the new thermal condition, and approaches the isothermal 1070 °C reference at $\varepsilon_{eq} = 0.55$, and finally ends at almost the same level. The system thus has enough strain at the higher temperature for DRX to adapt to the new condition.

For the later switches at $\varepsilon_{eq} = 0.4$ and 0.6, the situation is different. Here, the temperature change occurs after the isothermal 1020 °C curve has already crossed its critical value. This means that DRX has already been activated. As a result, when the temperature is increased to 1070 °C, $\bar{\rho}$ is well above ρ_{cr} of 1070 °C and DRX can still proceed, but the remaining strain interval is relatively short and part of the stored energy has already been consumed by DRX at 1020 °C. The non-isothermal curves bend downwards after the change, indicating that recovery and DRX reduce the stored dislocation density, but they do not converge to the isothermal 1070 °C reference. Instead at the final strain $\bar{\rho}$ remains slightly higher, with values of $\bar{\rho}$ = 3.51E+08 mm^{-2} for the temperature increase at ε_{eq}= 0.4 and $\bar{\rho}$ = 3.66E+08 mm^{-2} for the temperature increase at ε = 0.6, compared to $\bar{\rho}$ = 3.35E+08 mm^{-2} for the isothermal 1070 °C case. This corresponds to an increase of about 4 % (temperature increase at ε_{eq} = 0.4) and 6 % (temperature increase at ε_{eq} = 0.6), quantifying the slower and incomplete adaptation when the temperature increase is applied in the softening regime.

In the cooling paths in Figure 4 (b) the system starts from a high temperature DRX regime and is then transferred to a cooler state with reduced recovery and grain-boundary mobility. All three non-isothermal curves initially follow the isothermal 1120 °C reference. In all three cases $\bar{\rho}$ crosses the critical level ρ_{cr} of 1120 °C already at ε = 0.15, so that DRX is active at 1120 °C before the temperature change. When the temperature is reduced to 1070 °C, ρ_{cr} jumps to the higher value of ρ_{cr} = 3.5E+08 mm^{-2}, and the further evolution of $\bar{\rho}$ depends on the switching strain. For a change at ε_{eq}= 0.2, $\bar{\rho}$ is 2.4E+08 mm^{-2} at the onset of cooling. During the subsequent deformation, $\bar{\rho}$ increases gradually and reaches $\bar{\rho}$ = 3.7E+08 mm^{-2}, clearly above ρ_{cr}, implying an interval during which nucleation is suppressed before it resumes once $\bar{\rho}$ exceeds ρ_{cr}. This triggers a second DRX episode at the lower temperature, after which $\bar{\rho}$ decreases slightly and approaches a plateau close to the isothermal 1070 °C curve. If the change is delayed to ε_{eq}= 0.4, cooling occurs in the softening regime of the 1120 °C curve with $\bar{\rho}$ = 2.4E+08 mm^{-2} < ρ_{cr} of 1070 °C. Immediately after cooling no abrupt increase in DRX activity occurs and the curve evolves into a flat plateau. This indicates that most of the DRX has already taken place at 1120 °C, and the second stage mainly adjusts the microstructure towards a steady-state at 1070 °C without strongly modifying the overall DRX fraction. For the latest change at ε_{eq}= 0.6, the temperature decrease is applied at a late deformation stage at 1120 °C, where DRX has already reduced $\bar{\rho}$ to 2.1E+08 mm^{-2}, slightly below ρ_{cr} of 1120 °C. After the temperature change the non-isothermal curve rises and reaches $\bar{\rho}$ = 3.3E+08 mm^{-2}, but remains below ρ_{cr} of 1070 °C over the entire remaining strain range. It runs parallel to, but under, the isothermal curve of the new temperature of 1070 °C, ending at $\bar{\rho}$ = 3.14E+08 mm^{-2} compared to $\bar{\rho}$ = 3.35E+08 mm^{-2}.

This behavior suggests that, after the late temperature change, no further DRX is triggered at 1070 °C, the microstructure is already recrystallized and never fully adapts to the new conditions.

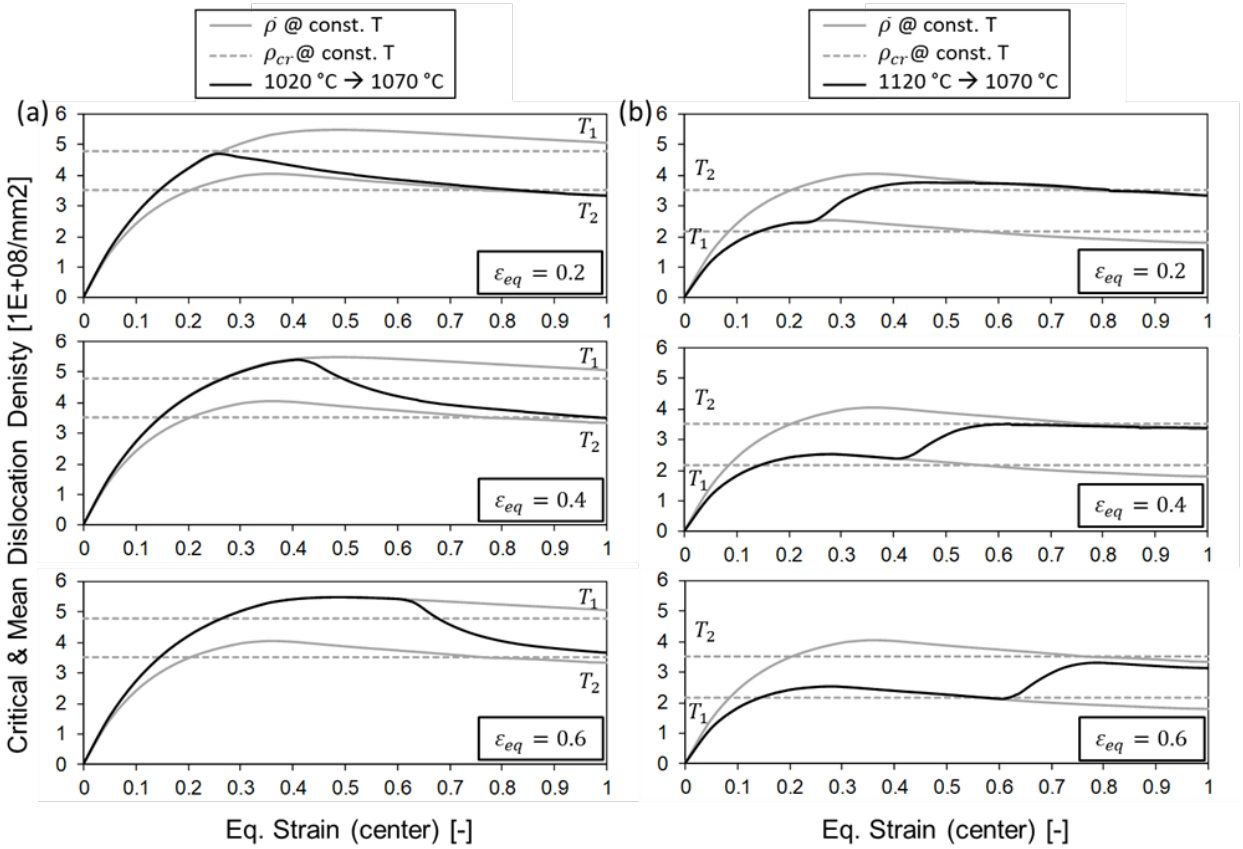

Fig. 4. Evolution of the critical and mean dislocation density during (a) temperature increase from 1020 °C to 1070 °C at equivalent strains 0.2, 0.4 and 0.6 and (b) temperature decrease at 0.2, 0.4 and 0.6

Microstructure Evolution. Figure 5 combines the evolution of the critical and mean dislocation density with the simulated microstructure for a temperature decrease at ε_{eq} = 0.6. The points a-d make four selected strain levels along the non-isothermal curve with the corresponding microstructures. At an equivalent strain in the specimen center of ε_{eq} = 0.4 DRX is active and the microstructure consists of deformed grains with few RX nuclei. At the change point ε_{eq}= 0.6 the microstructure is largely recrystallized. After the change ε_{eq} = 0.8 the microstructure shows further straining and growth of existing RX nuclei, rather than new DRX grains. In the final state ε_{eq} = 1.0 the microstructure is similar to that at ε_{eq} = 0.8. DRX occurs only at 1120 °C and during the stage at 1070 °C mainly the existing grains grow without a second recrystallization event.

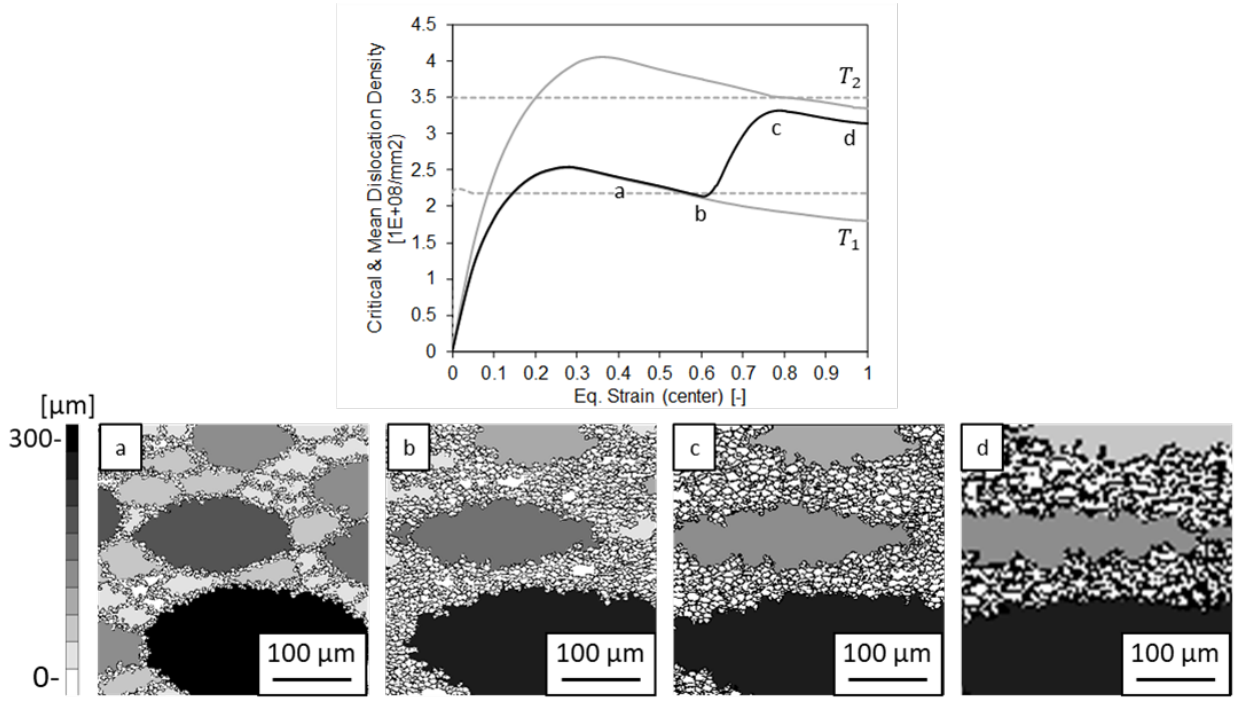

Fig. 5. Simulated intermediate microstructure states for the temperature decrease from 1120 °C to 1070 °C at ε = 0.6. Points a-d mark selected strains along the non-isothermal path at (a) ε_{eq}= 0.4, (b) ε_{eq} = 0.6, (c) ε_{eq}= 0.8 and (d) ε_{eq}= 1.0

Comparison of Experimental and Simulated Microstructures and Grain Size Distributions. The final microstructures for the temperature increase cases from 1020 °C to 1070 °C are shown in Figure 6 for (a) an early temperature change at ε = 0.2, (b) a change at ε = 0.4 and (c) a later change at ε = 0.6. The left image shows the experimental microstructure, the middle the corresponding DIGIMU® microstructure, and the right panel the experimental and simulated grain size distribution. For ε = 0.2 (Figure 6 (a)), the experimental microstructure (left) is dominated by fine recrystallized grains, with only a weak tail to larger diameters. The simulated microstructure (middle) exhibits a very similar microstructure consisting of deformed stretched grains and RX grains. The experimental grain size distribution exhibits a peak in the lowest grain size classes, with a large fraction of grains located at 10 µm. The simulated grain size distribution peaks at 14.5 µm. The corresponding grain size distributions reflect reduced refinement when more deformation occurs at 1020 °C before a temperature increase. For the change at ε = 0.4, both experiment and simulation display a coarser more heterogeneous grain structure compared to ε = 0.2. For the latest change at ε = 0.6 (Figure 6 (c)) the trend continues, both experiment and simulation display larger grains and the corresponding grain size distributions show a shift towards larger grain sizes.

The final microstructures for the temperature decrease from 1120 °C to 1070 °C are shown in Figure 7 for a change at (a) ε = 0.2, (b) ε = 0.4, and (c) ε = 0.6. For an early temperature change at ε = 0.2 (Figure 7 (a)), both experiment and simulation are filled with fine RX grains and smaller stretched deformed grains. The grain size distributions peak in the smallest classes at 20 µm in the experiment and 14.5 µm in the simulation. This reflects the underlying mechanism, DRX starts at 1120 °C and after the temperature decrease continues at 1070 °C. The additional DRX at 1070 °C leads to further grain refinement, which is consistently captured by the simulation and experiment. For the temperature decrease at ε = 0.4 (Figure 7 (b)), the experimental and simulated microstructure remains largely recrystallized. The peak of the grain size distributions still lies in the smallest class, but the peak surface fraction decreases to about 0.45, indicating that DRX at 1070 °C still contributes to refinement, yet less effectively than in the temperature decrease case at ε = 0.2. For the later temperature decrease at ε = 0.6 (Figure 7 (c)) the microstructure at the end of deformation shows larger deformed stretched grains with small RX grains. The grain size distribution still peaks at the

smaller classes, but the surface fraction is reduced to 0.45. In this case DRX proceeds entirely at 1120 °C and no significant additional DRX occurs at 1070 °C consistent with the dislocation density evolution discussed above.

Taken together Figure 6 and Figure 7 demonstrate that the timing and direction of the temperature change provide a microstructural control, while the DIGIMU® simulations reproduce these trends in good agreement with the experiments.

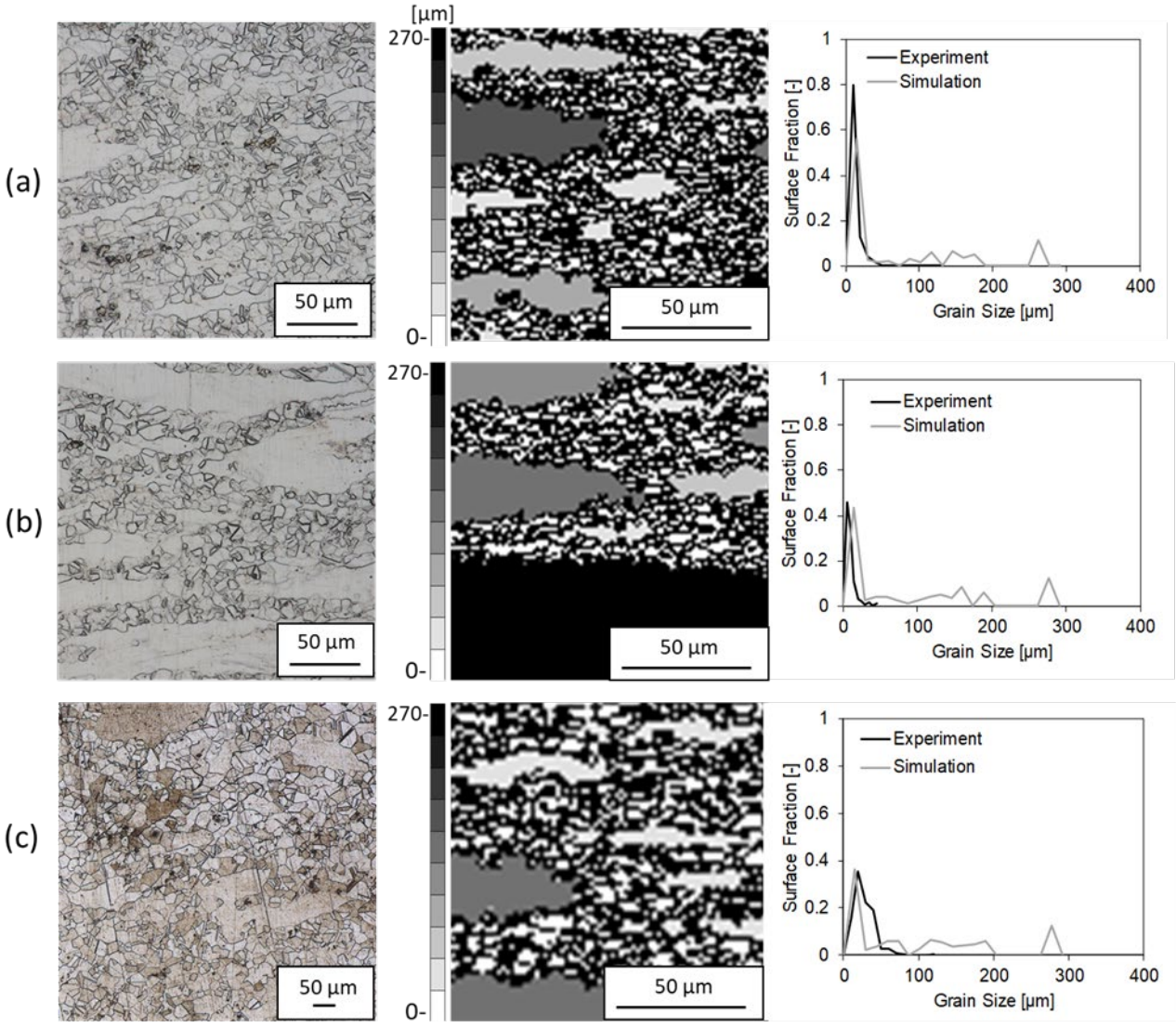

Fig. 6. Comparison of experimental (left) and simulated (middle) microstructures and grain size distribution (right) for a temperature increase at (a) ε = 0.2, (b) ε = 0.4 and (c) ε = 0.6

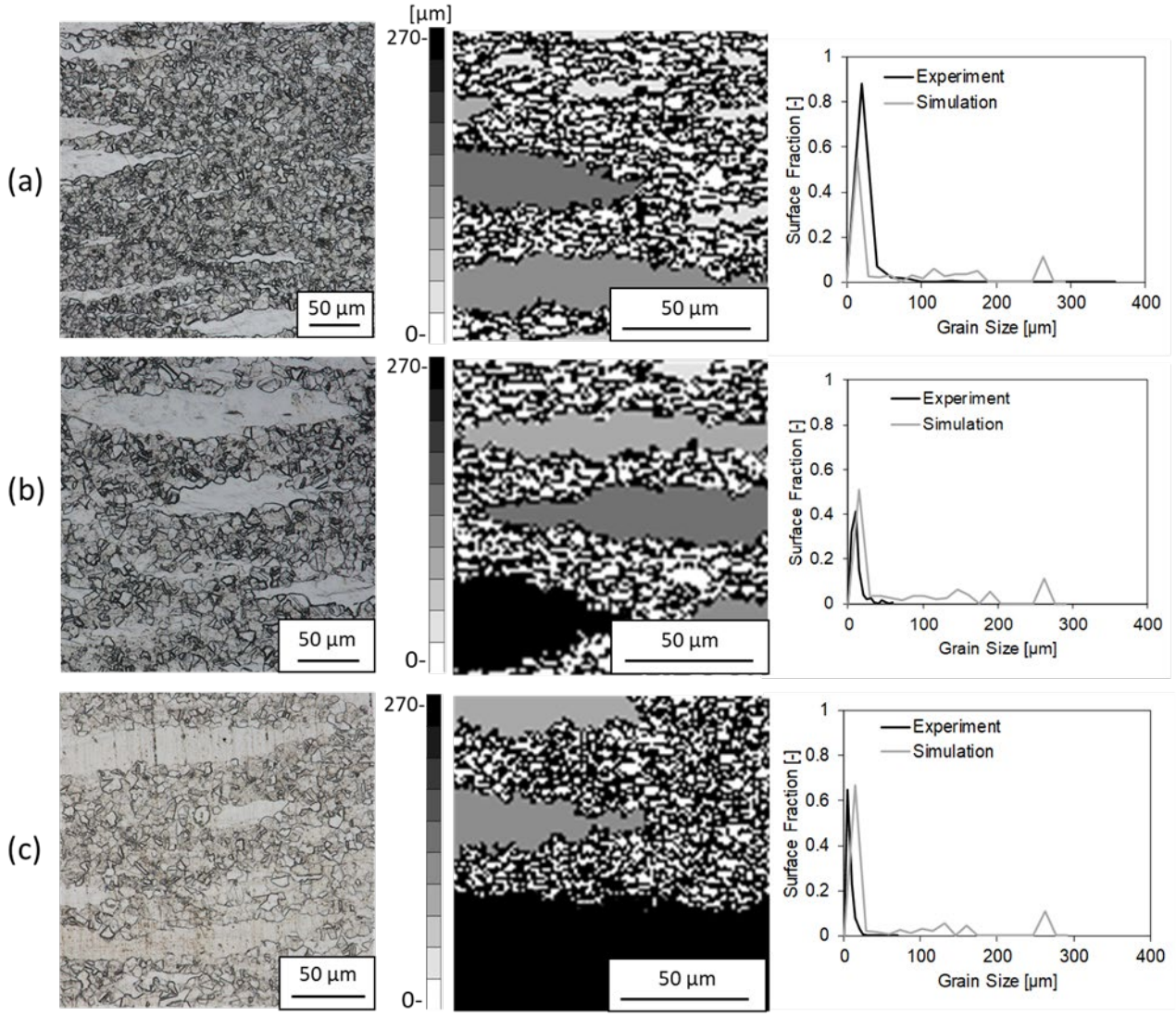

Fig. 7. Comparison of experimental (left) and simulated (middle) microstructures and grain size distribution (right) for a temperature decrease at (a) ε = 0.2, (b) ε = 0.4 and (c) ε = 0.6

Comparison of Experimental and Simulated DRX-Fractions. The final DRX-fractions for the transient temperature tests are compared for experiment and DIGIMU® simulations in Figure 8. For the temperature increase (Figure 8 (a)) both experiment and simulation indicate that an earlier temperature increase promotes a higher recrystallized fraction. At $\varepsilon = 0.2$, the experimental DRX is about 46 %, while the simulation predicts 55 %. When the temperature change is delayed to $\varepsilon = 0.4$, the DRX-fraction decreases 32 % in the experiment and 44 % in the simulation, and for $\varepsilon = 0.6$ it drops further to 23 % (experiment) and 37 % (simulation). An earlier temperature increase gives the material more strain at 1070 °C, where DRX proceeds more rapidly. In contrast, a later change allocates more deformation to 1020 °C, where DRX is less pronounced, so that a smaller fraction of the microstructure can recrystallize.

For the temperature decrease (Figure 8 (b)), experiment and simulation show similar behavior. At $\varepsilon = 0.2$, the experimental DRX-fraction is 50 % while the simulation predicts 54 %. At $\varepsilon = 0.4$, the DRX fractions remain at a similar level, 49 % in the experiment and 51 % in the simulation. When the temperature decrease is applied at $\varepsilon = 0.6$, the corresponding values are 55 % (experimental) and 66 % (simulative). A later temperature decrease produces a somewhat higher DRX-fraction, since more deformation is applied at 1120 °C, where DRX is effective, before the material is transferred to 1070 °C. This behavior is consistent with the dislocation density and microstructure analyses, which

showed that DRX is already well advanced during high temperature stage and that the deformation at 1070 °C mainly preserves and slightly adjusts the existing recrystallized structure.

Overall the comparison in Figure 8 shows that the DIGIMU® simulations captures the main features of the experimental DRX behavior under both temperature increase and decrease conditions. The deviations are typically on the order of 5-10 %, with tendency to overestimate DRX. This can partly be attributed to the experimental measurement by the line-intercept method on microstructure pictures that were taken with optical microscope, where small recrystallized grains may be missed, while the simulation counts all recrystallized regions in the RVE.

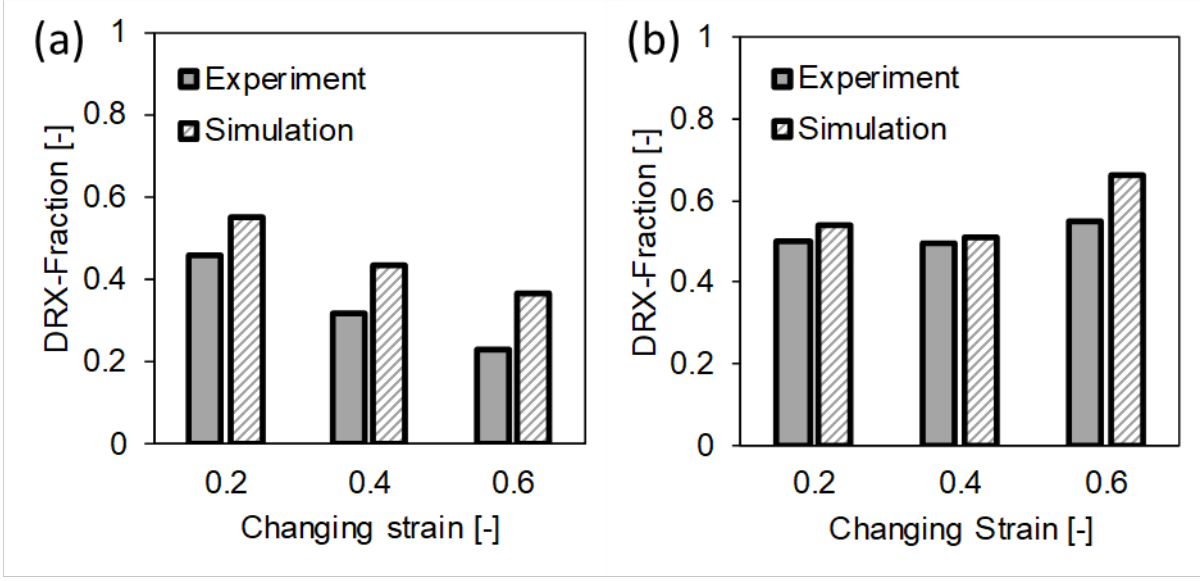

Fig. 8. Comparison of final DRX-fraction between experiment and simulation for (a) temperature increase from 1020 °C to 1070 °C at strains ε = 0.2, 0.4 and 0.6; and (b) temperature decrease from 1120 °C to 1070 °C at strains ε = 0.2, 0.4 and 0.6

Conclusions.

In this work, the influence of transient temperature paths during hot deformation on the microstructure evolution of Inconel 718 was investigated by combining dilatometer tests with Full-Field simulations in DIGIMU®. Non-isothermal compression tests with temperature increases (1020 °C to 1070 °C) and decreases (1120 °C to 1070 °C) were performed, with the temperature change imposed at different strains. The measured temperature-time curves were directly imposed in the simulations. Isothermal tests at 1020 °C, 1070 °C and 1120 °C served as reference. The results show a pronounced path dependence. Early heating to 1070 °C yields higher DRX fractions and finer, more homogeneous grain structures, while later heating leaves less strain at the higher temperature and produces coarser, less recrystallized microstructures. For cooling, DRX takes place mainly at 1120 °C. After an early temperature change, DRX can continue at 1070 °C, whereas a late change transfers an almost fully recrystallized state into a regime where further DRX is suppressed. These mechanisms are consistently reflected in dislocation density evolution, final DRX fractions and grain size distributions.

References

[1] R. Bobbili, V. Madhu, An investigation into hot deformation characteristics and processing maps of high-strength armor steel, Journal of Materials Engineering and Performance 24 (2015) 4728–4735.

[2] S. Spigarelli, A. Jäger, M. El Mehtedi, V. Gärtnerová, Microstructural and constitutive analysis in process modeling of hot working: The case of a Mg-Zn-Mn alloy, Materials Science and Engineering: A 661 (2016) 40–50.

[3] M. Hasan Nasab, S. Serajzadeh, Thermal stresses and kinetics of phase transformation on the run-out table after hot strip rolling of low-carbon steels, The International Journal of Advanced Manufacturing Technology 83 (2016) 1725–1736.

[4] F. Qin, Y. Li, H. Qi, X. Wei, Microstructure and mechanical properties of as-cast 42CrMo ring blank during hot rolling and subsequent quenching and tempering, Journal of Materials Engineering and Performance 26 (2017) 1300–1310.

[5] H. Zhang, C. Li, Y. Liu, Q. Guo, H. Li, Precipitation behavior during high-temperature isothermal compressive deformation of Inconel 718 alloy, Materials Science and Engineering: A 677 (2016) 515–521.

[6] Y.C. Lin, F.-Q. Nong, X.-M. Chen, D.-D. Chen, M.-S. Chen, Microstructural evolution and constitutive models to predict hot deformation behaviors of a nickel-based superalloy, Vacuum 137 (2017) 104–114.

[7] P. Zhang, C. Yi, G. Chen, H. Qin, C. Wang, Constitutive model based on dynamic recrystallization behavior during thermal deformation of a nickel-based superalloy, Metals 6 (2016) 161.

[8] S.S. Satheesh Kumar, T. Raghu, P.P. Bhattacharjee, G. Appa Rao, U. Borah, Constitutive modeling for predicting peak stress characteristics during hot deformation of hot isostatically processed nickel-base superalloy, Journal of Materials Science 50 (2015) 6444–6456.

[9] N.V. Jagtap, N. Reinisch, R. Abdusalamov, D. Bailly, M. Itskov, Modeling of equivalent strain in 2D cross-sections of open die forged components using neural networks, Advances in Industrial and Manufacturing Engineering 9 (2024) 100152.

[10] Y.C. Lin, F. Wu, Q.-W. Wang, D.-D. Chen, S.K. Singh, Microstructural evolution of a Ni-Fe-Cr-base superalloy during non-isothermal two-stage hot deformation, Vacuum 151 (2018) 283–293.

[11] B. Scholtes, M. Shakoor, A. Settefrati, P.-O. Bouchard, N. Bozzolo, M. Bernacki, New finite element developments for the full field modeling of microstructural evolutions using the level-set method, Computational Materials Science 109 (2015) 388–398.

[12] P.O. de Micheli, L. Maire, D. Cardinaux, C. Moussa, N. Bozzolo, M. Bernacki, DIGIMU®: Full field recrystallization simulations for optimization of multi-pass processes, in: PROCEEDINGS OF THE 22ND INTERNATIONAL ESAFORM CONFERENCE ON MATERIAL FORMING: ESAFORM 2019, AIP Publishing, 2019, p. 40014.

[13] B. Flipon, N. Bozzolo, M. Bernacki, A simplified intragranular description of dislocation density heterogeneities to improve dynamically recrystallized grain size predictions, Materialia 26 (2022) 101585.

[14] A. Yoshie, H. Morikawa, Y. Onoe, K. Itoh, Formulation of static recrystallization of austenite in hot rolling process of steel plate, Transactions of the Iron and Steel Institute of Japan 27 (1987) 425–431.

[15] DIN EN ISO 643: 2013-05, Stahl - Mikrophotographische Bestimmung der erkennbaren Korngröße (ISO_643:2012): Deutsche Fassung.

[16] H. Brüggemann, A. Quadfasel, J.A. Nietsch, M. Teller, P. de Micheli, B. Flipon, M. Bernacki, Korngrößenvorhersage beim Freiformschmieden von Inconel 718 mit DIGIMU®, massivUMFORMUNG 2021 (2021) 50–54.

[17] J. Agirre, D. Bernal, B. Flipon, M. Bernacki, H. Brüggemann, D. Bailly, M. Merklein, H. Hagenah, J.H. Risse, Ł. Madej, K. Muszka, K. Cichocki, Ł. Poloczek, O. Bylya, A. Reshetov, P. de Micheli, J. Barlier, A. Stark, U.F.H. Suhuddin, P. Staron, B. Klusemann, L. Galdos, The ESAFORM benchmark 2023: interlaboratory comparison benchmark for the characterization of microstructural grain growth and dynamic recrystallization kinetics of a single-phase Ni-base superalloy, Int J Mater Form 18 (2025).

The publication of this article was funded by the RWTH Aachen University 10.13039/501100007210